第 43 卷 第 7 期/2023 年 4 月/光学学报 研究论文

光学学报

基于内调制DFB激光器的高空间分辨率TGD-OFDR

戴建平[1]，邱锦波[1]，刘宏睿[1]，罗一民[1,2*]，刘庆文[2]

[1]中煤科工集团上海有限公司，上海 200030；

[2]上海交通大学区域光纤通信网与新型光通信系统国家重点实验室，上海 200240

摘要 提出了一种利用内调制频率调谐实现高空间分辨率的时间门控数字光频域反射仪(TGD-OFDR)方案，采用电流调谐的分布式反馈(DFB)二极管激光器作为探测光源提供较大的激光频率调谐范围的信号，利用马赫-曾德尔干涉仪(MZI)分析该DFB激光器的电流-频率响应特性后，由任意波形发生器产生的带有预失真的锯齿波信号驱动该DFB激光器，进而补偿激光器扫频时的非线性，同时采用一台波长可调节的稳频激光器的出射光充当本地稳频参考光。实验测试在74 km的光纤链路上实现了10 cm的空间分辨率，动态范围为23.3 dB。

关键词 传感器；光纤测量；时间门控数字光频域反射仪；分布式反馈激光器；预失真

中图分类号 TP212 **文献标志码** A **DOI**：10.3788/AOS221629

1 引 言

光反射仪技术是分布式光纤传感器的一项重要技术。在光通信网络等应用领域中，光反射仪需要同时满足长距离测量和高空间分辨率的功能。光时域反射仪(OTDR)是广泛应用于远程光纤链路测量的方法之一[1]，其测量距离可达数百千米。但OTDR的空间分辨率受动态范围的限制[2]，功率放大[3]、波长编码[4]等方法仍难以将动态范围提高至满意的范围，因此最终只能在动态范围和空间分辨率之间进行权衡。

相干光频域反射仪(C-OFDR)[5]是另一种典型的光反射仪，其空间分辨率取决于扫频范围，可以同时提供高空间分辨率和大动态范围[6]。但是，由于激光光源的相位噪声[7]和扫频的线性度[8]，C-OFDR的探测范围受到光源线宽的限制，一旦探测距离接近激光器相干长度，信噪比(SNR)就会出现严重的退化[9-13]。抑制相位噪声是解决激光器相干长度限制问题的方法之一。时间门控数字光频域反射仪(TGD-OFDR)技术利用高激光啁啾率来抑制激光源的相位噪声的影响，实现了超过激光相干长度的长距离探测[14]。TGD-OFDR系统的空间分辨率由探测脉冲的频率调制范围决定，现有的TGD-OFDR系统均采用外调制方案，其探测脉冲频率调谐范围较小，一般将系统的空间分辨率限制在米级水平。分布式反馈(DFB)二极管激光器具有良好的单模工作特性，且其发射激光的频率可以通过改变驱动电流而得到大范围快速调谐，具有作为TGD-OFDR系统的探测光的潜力。然而，DFB二极管激光器固有的非线性频率响应是实现线性扫频所面临的一个严峻挑战，如何解决非线性问题成为一个难题[15-20]。

本文提出了一种改进的TGD-OFDR，采用具有内部调谐功能的DFB激光器作为光源，利用马赫-曾德尔干涉仪(MZI)测量DFB激光器的调谐非线性，反馈系统可以对激光器驱动信号的波形进行预处理，实现线性的频率扫描，利用激光高啁啾率优势来抑制相位噪声。系统采用一台窄线宽激光器为相干探测提供稳定的本地光，实现对后向散射信号的相干检测；同时，可利用探测光脉冲与本地光直接拍频得到的拍频信号产生匹配滤波信号，实现对后向散射信号的解调，实现74 km光纤链路上10 cm级空间分辨率的探测。

2 基本原理

2.1 TGD-OFDR

TGD-OFDR系统的基本原理图如图1所示。文献[14]中对TGD-OFDR技术的理论进行了详细的介绍，在本文中只做简单介绍。来自激光光源的光波通过耦合器被分成两束光，其中一束作为探测光，由声光调制器(AOM)在函数发生器(FG)的驱动下进行扫频

收稿日期：2022-08-22；**修回日期**：2022-10-13；**录用日期**：2022-10-19；**网络首发日期**：2022-10-29

基金项目：中煤科工集团上海有限公司科技开发项目(017819)

通信作者：*luo_yimin@163.com

和切脉冲，得到啁啾脉冲，而本地参考光为频率稳定的连续光波。

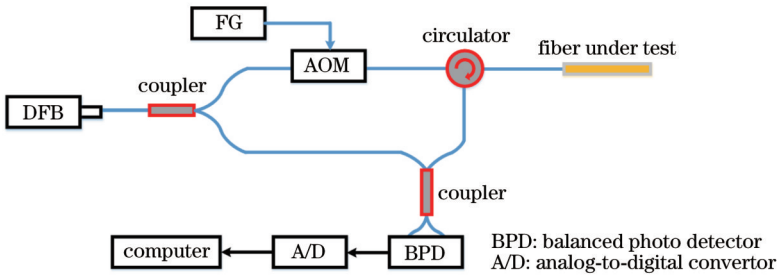

图 1　TGD-OFDR 系统框图

Fig. 1　Schematic diagram of TGD-OFDR system

经过 AOM 后的探测光为一个啁啾脉冲，其光电场与脉冲带宽 τ_p 和线性扫频速率 γ 的关系为

$$E_p(t)=\mathrm{rect}\left(\frac{t}{\tau_p}\right)E_0\exp\left[\mathrm{j}\left(2\pi f_0 t+\pi\gamma t^2\right)\right],\quad(1)$$

式中：rect(·)为矩形窗函数；E_0 为初始光电场强度；f_0 为初始频率。啁啾信号的频率范围为 $\Delta f=\gamma\tau_p$。

待测光纤内不同位置的反射光电场表达式为

$$E_{\mathrm{reflect},\tau_d}(t)=\mathrm{rect}\left(\frac{t-\tau_d}{\tau_p}\right)\sqrt{R}\,E_0\exp\left\{\mathrm{j}\left[2\pi f_0(t-\tau_d)+\pi\gamma(t-\tau_d)^2\right]\right\},\quad(2)$$

式中：τ_d 为相对参考光的延迟；R 为待测光纤内时延为 τ_d 位置处的反射率。

参考光为连续光波，恒定频率为 f_0，本地光电场 $E_{\mathrm{loc}}(t)$ 的表达式为

$$E_{\mathrm{loc}}(t)=E_{\mathrm{loc}}\exp\left[\mathrm{j}\left(2\pi f_0 t\right)\right],\quad(3)$$

式中：E_{loc} 为初始本地参考光的电场强度。时延为 τ_p 的反射光和参考光在平衡探测器(BPD)中相干，得到的电流信号(忽略直流分量)为

$$I_{\mathrm{eat},\tau_d}(t)=\mathrm{rect}\left(\frac{t-\tau_d}{\tau_p}\right)2\sqrt{R}\,E_0E_{\mathrm{loc}}\cos\left[\pi\gamma(t-\tau_d)^2-2\pi f_0\tau_d+\theta(t)\right],\quad(4)$$

式中：$\theta(t)$ 为激光相位噪声项。由式(4)可知，拍频信号也是一种具有相同扫频速率 γ 和扫频范围 Δf 的啁啾信号。

为了在解调拍频信号后获得待测光纤的位置信息，在数字域中产生一个如图 2 所示的等效参考量 $S_{\mathrm{ref}}(t)=\cos\left(\pi\gamma t^2\right)$。

2.2　DFB 激光器的预失真系统

本文系统采用电流调谐的 DFB 激光器作为内调制光源，为了提高直接调谐的 DFB 激光器扫频线性度，提出了一个预反馈失真系统。在这种方法中，需要监测频率随时间的变化，用马赫-曾德尔干涉仪监测扫频状态随时间的变化，对所得到的拍频信号进行希尔伯特变换以得到扫频信号的瞬时频率变化信息[21]。

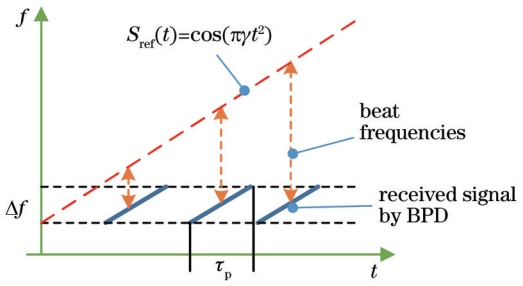

图 2　平衡探测器接收到的拍频信号和等效参考信号

Fig. 2　Beat signals received by BPD and equivalent reference signal

设激光器发出的信号为 $a_0(t)$：

$$a_0(t)=|a_0|\exp\left[\mathrm{j}\varphi(t)\right],\quad(5)$$

式中：$|a_0|$ 为信号振幅；$\varphi(t)$ 为信号随时间变化的相位信息。

瞬时光学频率为相位信息的微分，可得

$$v_0(t)=\left(\frac{1}{2\pi}\right)\frac{\mathrm{d}\varphi(t)}{\mathrm{d}t}。\quad(6)$$

平衡探测器接收到的马赫-曾德尔干涉仪单反射点的干扰信号为

$$y(t)=y_0\cos\left[\varphi(t)-\varphi(t-\tau)+\xi_0\right],\quad(7)$$

式中：y_0 为电流强度信息；ξ_0 为恒定相位项；τ 为延迟时间。

对 $\varphi(t-\tau)$ 进行泰勒展开，可得

$$\varphi(t-\tau)=\frac{\varphi(t)}{0!}+\frac{\varphi'(t)}{1!}(-\tau)+\frac{\varphi''(t)}{2!}(-\tau)^2+\cdots,\quad(8)$$

式中：$\varphi'(t)$、$\varphi''(t)$ 分别为 $\varphi(t)$ 的一阶和二阶微分。当延迟时间足够小(约小于 1 ns)、扫频速率足够大(大于 100 GHz/s)时，可得

$$\varphi(t)-\varphi(t-\tau)\approx\tau\varphi'(t)=2\pi\tau v(t),\quad(9)$$

故式(7)可简化为

$$y(t)=y_0\cos\phi(t),\quad(10)$$

式中：$\phi(t)=2\pi\tau v(t)+\xi_0$。使用希尔伯特变换提取 $y(t)$ 的相位信息[22]：

$$H\{y(t)\}=y_0\sin\phi(t),\tag{11}$$

$$\phi(t)=\arctan\frac{y(t)}{H\{y(t)\}},\tag{12}$$

$$v_0(t)=\frac{1}{2\pi\tau}\left\{\arctan\frac{y(t)}{H\{y(t)\}}-\xi_0\right\}=\frac{1}{2\pi n}\cdot\frac{c}{\Delta L}\left\{\arctan\frac{y(t)}{H\{y(t)\}}-\xi_0\right\},\tag{13}$$

式中：c为真空中光速；ΔL为干扰信号点到激光源的距离；n为光纤折射率。

补偿算法选用工程中常用的比例积分微分（PID）算法[23]，算法流程图如图3所示。

根据图3，需要在计算机中生成参考时频函数$v_{ideal}(t)$，通过与$v_0(t)$比较，得到差错信号$v_{err}(t)$。通过PID算法可以得到补偿信号$\mu(t)$：

$$\mu(t)=K_p v_{err}(t)+K_i\int_0^t v_{err}(\tau)\mathrm{d}\tau+K_d\frac{\mathrm{d}v_{err}(t)}{\mathrm{d}t},\tag{14}$$

式中：K_p为比例系数；K_i为积分系数；K_d为微分系数。K_p、K_i与K_d统称为设定点，不能通过特定公式求得，而是需要根据结果进行实时调整，它们的取值直接决定了PID算法的调节效果。

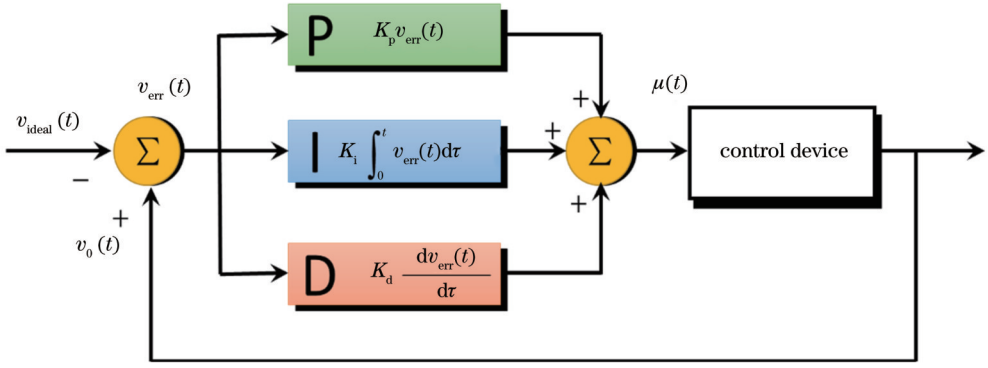

图3　PID算法流程图

Fig. 3　Flow chart of PID algorithm

3　实验测试与分析

3.1　预失真系统

作为前提条件，在对DFB激光器的电流进行调制时，首先对非线性扫频信号进行补偿。整个预失真系统由马赫-曾德尔干涉仪与反馈部分组成，具体实现与计算过程如图4所示。

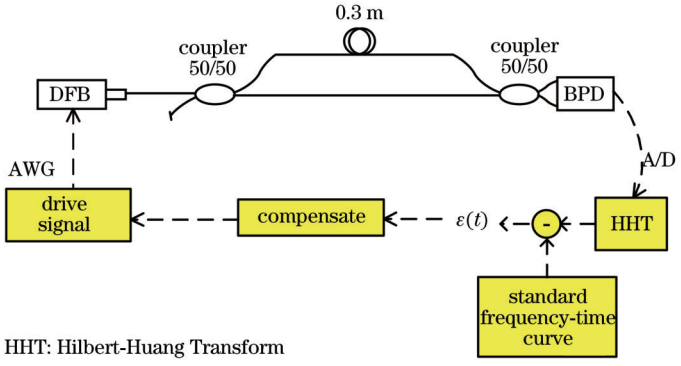

图4　预失真系统与计算过程

Fig. 4　Pre-distortion system and calculation process

马赫-曾德尔干涉仪的一路为约0.3 m的延迟光纤，这使得式(9)成立。预失真系统为闭环反馈系统，具体的运行步骤分为：

1）驱动DFB激光器。计算机控制任意波形发生器（AWG，NI PXI-5422），产生初始电流波形$V_0(t)$，以调制DFB激光器。

2）从马赫-曾德尔干涉仪中获取信号。DFB激光器所发射出的激光进入光纤长度差为0.3 m的马赫-曾德尔干涉仪系统中。通过BPD（PDB480C）与模拟-数字转换器（ADC）采集拍频信号后输入计算机中。

3）计算与补偿。通过希尔伯特变换得出初始时频函数，利用PID补偿算法得到新的驱动信号$V_1(t)$。

4）重复。利用$V_1(t)$重复步骤1）～3），直到$v_n(t)$具有合适的线性度为止，得到最终的驱动信号$V_{fin}(t)$。

DFB激光器预失真结果图如图5所示。当DFB激光器直接施加锯齿波扫频信号时，在25 μs的时间内

实现了 10 GHz 左右的扫频范围，扫频速率高达 400 THz/s，但非线性程度严重，最大频偏达到了 1.2 GHz，如图 4(a)所示。

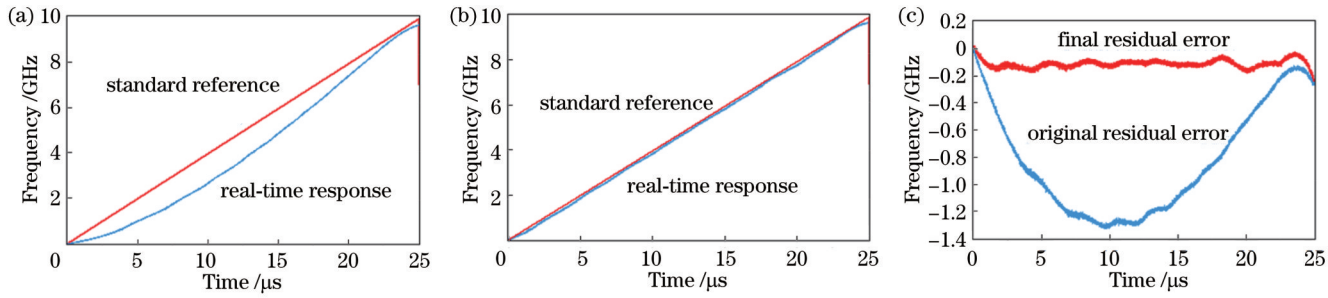

图 5　DFB 激光器的预失真实验结果。(a)原始时频曲线，25 μs 内扫频范围为 10 GHz；(b)预失真之后的时频曲线；(c)预失真前后的差错信号曲线

Fig. 5　Results of predistortion experiments of DFB laser. (a) Original time-frequency curve (10 GHz sweep frequency range within 25 μs); (b) time-frequency curve after pre-distortion; (c) residual error curves before and after pre-distortion

经过上述预失真的电流信号调制后，DFB 激光器的拍频信号的线性度有了显著提升，如图 5(b)所示。预失真前后差错信号的曲线图如图 5(c)所示。预失真后的曲线虽距频率轴为 0 的水平线有 100 MHz 的频差，但水平度较好，表明线性程度得到了改善，其频率抖动的范围只有约 40 MHz。后续可采用更精细的预失真算法与更高精度的 DAQ 与 AWG 装置对该系统进行进一步优化。

3.2　基于 DFB 的 TGD-OFDR 系统

实验系统框图如图 6 所示。

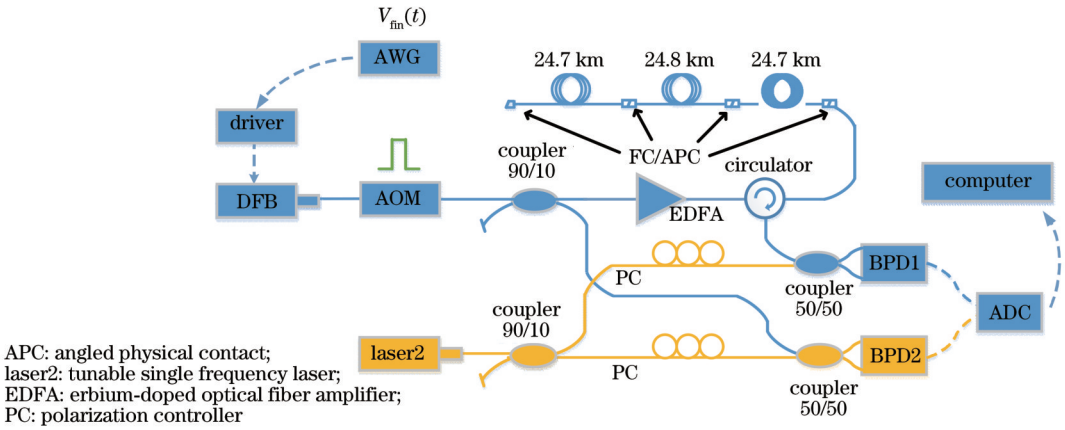

图 6　基于 DFB 内调制的 TGD-OFDR 系统框图

Fig. 6　Schematic diagram of TGD-OFDR system based on internally modulated DFB

使用调制好的电压信号 $V_{fin}(t)$ 作为 DFB 激光器的调制信号，DFB 激光器发出的激光经过 AOM 斩波后，得到脉冲带宽为 τ_p、线性扫频速率为 γ 的啁啾脉冲，啁啾脉冲公式如下：

$$E_{DFB}(t)=\mathrm{rect}\left(\frac{t}{\tau_p}\right)E_1\exp\left[\mathrm{j}\left(2\pi f_1 t+\pi\gamma t^2\right)\right],\quad(15)$$

式中：E_1 为振幅；f_1 为初始频率。$E_{DFB}(t)$ 通过 90∶10 耦合器得到两路信号：

$$E_{DFB,90}(t)=\mathrm{rect}\left(\frac{t}{\tau_p}\right)0.9E_1\exp\left[\mathrm{j}\left(2\pi f_1 t+\pi\gamma t^2\right)\right],\quad(16)$$

$$E_{DFB,10}(t)=\mathrm{rect}\left(\frac{t}{\tau_p}\right)0.1E_1\exp\left[\mathrm{j}\left(2\pi f_1 t+\pi\gamma t^2\right)\right]。\quad(17)$$

信号 $E_{DFB,90}(t)$ 作为探测脉冲进入待测光纤前，会经过掺铒光纤放大器(EDFA)的放大，对 $E_{DFB,10}(t)$ 则不进行任何处理。通过自外差法得出 DFB 激光器的扫频线宽为 4.5 MHz。

同时，使用线宽为 50 kHz 的可调谐单频激光器(laser2)作为本地参考稳频光，进行振幅 E_2、频率 f_2、相位 $\theta_2(t)$ 的相干检测。laser2 发出的信号同样经过 90∶10 耦合器分为两路：

$$E_{laser2,90}(t)=0.9E_2\exp\left\{\mathrm{j}\left[2\pi f_2 t+\theta_2(t)\right]\right\},\quad(18)$$

$$E_{laser2,10}(t)=0.1E_2\exp\left\{\mathrm{j}\left[2\pi f_2 t+\theta_2(t)\right]\right\}。\quad(19)$$

信号 $E_{laser2,10}(t)$ 和 $E_{DFB,10}(t)$ 会合后在 BPD 中产生一个模拟参考信号：

$$S_{\mathrm{Aref}}(t)=\mathrm{rect}\left(\frac{t}{\tau_{\mathrm{p}}}\right)\times 0.1\times 0.1\times E_1E_2\cos\left[\pi\gamma t^2+2\pi(f_1-f_2)t-\theta_2(t)\right]。\tag{20}$$

第2节中描述了在数字域中产生一个等效参考量$S_{\mathrm{ref}}(t)=\cos(\pi\gamma t^2)$的解调原理。此处采用$S_{\mathrm{Aref}}(t)$代替$S_{\mathrm{ref}}(t)$进行解调。来自待测光纤延迟$\tau$时间处的散射/反射光波与本地参考信号$E_{\mathrm{laser2,10}}(t)$会合，并被BPD接收，产生一个拍频信号：

$$I_{\tau}(t)=\mathrm{rect}\left(\frac{t-\tau}{\tau_{\mathrm{p}}}\right)\times 0.9\times 0.9\times 2\sqrt{R}\,E_{\mathrm{EDFA}}E_1E_2\cos\left[\pi\gamma(t-\tau)^2+2\pi(f_1-f_2)(t-\tau)-\theta_2'(t-\tau)\right],\tag{21}$$

式中：E_{EDFA}为EDFA的增益；$\theta_2'(t-\tau)$为激光在延迟时间τ处的相位函数。由式(20)、(21)可知，在$\theta_2(t)\approx\theta_2'(t-\tau)$时，laser2相位保持相对稳定，可得

$$KS_{\mathrm{Aref}}(t-\tau)=I_{\tau}(t),\tag{22}$$

式中：K为玻尔兹曼常数。

式(22)表明，$S_{\mathrm{Aref}}(t-\tau)$可以作为一个匹配滤波器，从散射/反射的光波$E_{\mathrm{reflect}}(t)$中滤除位置信息。互相关函数如下：

$$R_{\mathrm{SE}}(\tau)=S_{\mathrm{Aref}}(t)\otimes E_{\mathrm{reflect}}(t)=S_{\mathrm{Aref}}(-t)*E_{\mathrm{reflect}}(t),\tag{23}$$

$$R_{\mathrm{SE}}(\tau)=\lim_{T\to\infty}\frac{1}{T}\int_0^T S_{\mathrm{Aref}}(t)E_{\mathrm{reflect}}(t-\tau)\mathrm{d}t,\tag{24}$$

式中：$R_{\mathrm{SE}}(\tau)$为互相关函数；T为进行一次信号扫频和测量的周期；$\otimes$代表互相关运算；$*$代表卷积运算。

上述的TGD-OFDR系统采用模拟参考信号$S_{\mathrm{Aref}}(t)$作为匹配滤波器，从散射/反射光中解调待测光纤中的信号成分。但是由于互相关函数的特性，非线性扫频会对空间分辨率的性能造成影响。不同扫频线性度对相关运算空间分辨率影响的仿真结果如图7所示，其中图7(a)为4个具有相同扫频范围、不同扫频线性度信号的时间频率曲线，图7(b)为对应的相关运算分辨率结果图。

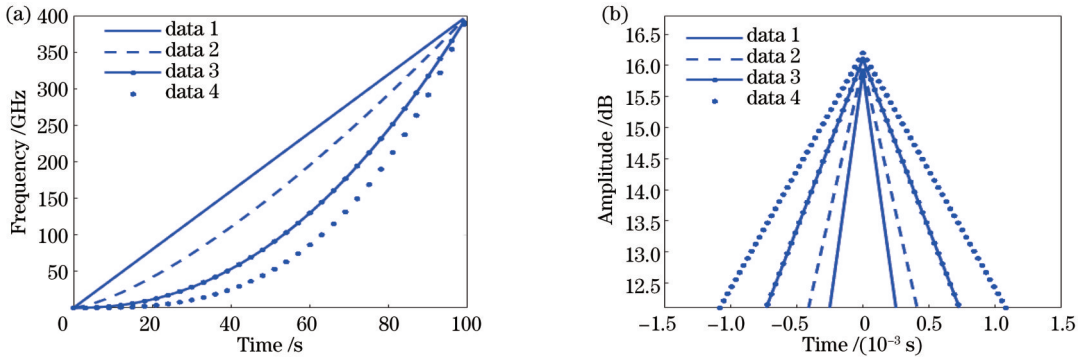

图7　不同扫频线性度对相关运算空间分辨率的影响。(a)不同扫频线性度信号的时频曲线；(b)不同扫频线性度信号对应的空间分辨率

Fig. 7　Effect of different sweep linearities on spatial resolution of correlation operation. (a) Time-frequency curves of sweep signals with different linearity; (b) spatial resolution corresponding to sweep signals with different linearity

由图7可得，线性扫频信号的线性度越高，其对应的空间分辨率就越高。因此，DFB激光器的线性度预失真可改善扫频非线性，进而提高反射仪系统的空间分辨率。

待测光纤尾端的空间分辨率降低的原因除了相位噪声之外，还有laser2的相位抖动。当频谱相关性逐渐降低时，解调结果会逐渐变差，仿真结果如图8所示。

由图8可知，若本地激光不稳定，使得$\theta_2(t)\neq\theta_2'(t-\tau)$时，$S_{\mathrm{Aref}}(t)$与$I_{\tau}(t)$的频谱相关性会降低，随着$\theta_2(t)$与$\theta_2'(t-\tau)$相差程度逐渐增大，互相关运算得到的结果也逐渐变差，直至无法解调。由于越远的探测光纤处反射回的光对应的时间延迟越长，laser2的相位同样也经历了较长时间，使得相位发生抖动。因此，laser2频率的稳定性直接影响了长距离探测的解调效果。

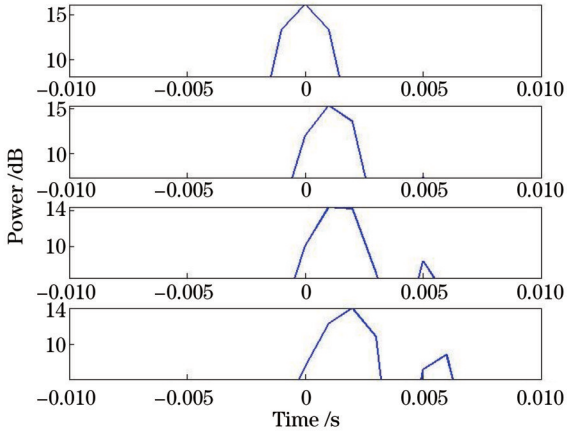

图8　频谱相关性对解调结果的影响

Fig. 8　Influence of spectrum correlation on demodulation results

3.3　实验结果与分析

实验中通过使用信号发生器控制AOM，将脉冲宽度 τ_p 设定为6 μs，啁啾脉冲信号的扫频范围约为1.1 GHz，理论空间分辨率可达9 cm。本地参考激光器是一个可调谐的单频二极管激光器。采用NI 5185 A/D采集卡对BPD接收的信号进行采样，采样率为6.25 GSa/s，分辨率为8 bit。待测光纤由3卷长分别为24.7 km、24.8 km和24.7 km的单模光纤组成。待测光纤的瑞利强度曲线如图9(a)所示。

在7种不同的激光波长下进行了2100次测量，平均后瑞利强度曲线的动态范围为23.3 dB。当激光器功率足够大时，动态范围还可以得到进一步的增大。待测光纤起始端的空间分辨率为10 cm，如图9(b)所示，与理论空间分辨率十分接近。待测光纤尾端的空间分辨率为18 cm，如图9(c)所示，空间分辨率有所降低，其主要原因是：随着探测距离的增加，laser2的相位抖动与相位噪声不断积累，且相位噪声远大于DFB激光器的线宽。从实验结果可以看出，虽然空间分辨率随着测量距离的增大有所降低，但由于调频范围足够大，仍比文献[14]中的空间分辨率高5倍左右。这也是目前已报道的探测长度超过60 km的OFDR所能达到的最高空间分辨率[24-26]。

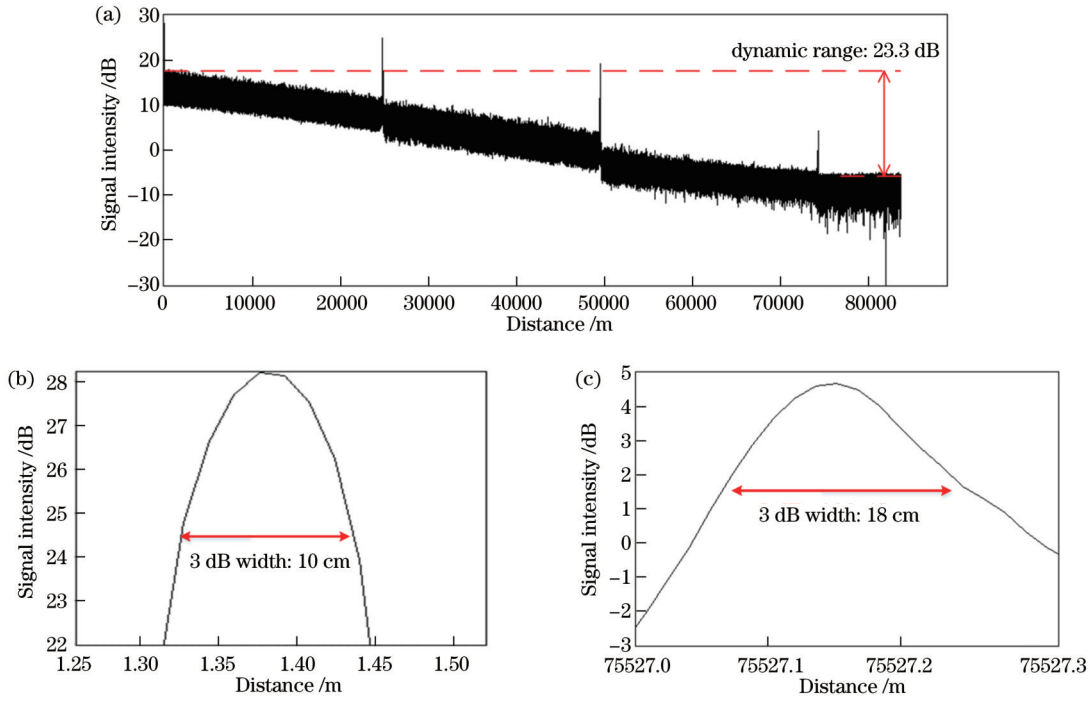

图9　基于DFB激光器的TGD-OFDR系统实验结果。(a) 74 km待测光纤(FUT)的瑞利强度曲线；(b)待测光纤起始端的空间分辨率；(c)待测光纤尾端的空间分辨率

Fig. 9　Experimental results of TGD-OFDR system based on DFB laser. (a) Rayleigh intensity curve over 74 km FUT; (b) spatial resolution at near end of FUT; (c) spatial resolution at far end of FUT

4　结　　论

采用内调制DFB激光器作为时间门控数字光频域反射系统的扫频光源，电流调制的DFB激光器具有1.1 GHz的频率调谐范围，且调谐速率较快，同时采用可调谐单频激光器即laser2作为本地参考稳频光。针对DFB激光器的调制方式和非线性扫频特性，设计了基于马赫-曾德尔干涉仪和PID算法的扫频非线性预失真系统。在74 km的待测光纤链路上，分别得到了起始端与末端10 cm、18 cm的空间分辨率，这是目前已报道的、探测长度超过60 km的OFDR所能达到的最高空间分辨率。未来可通过更精确的预失真算法、更稳定的本地参考光和更大功率的光源，进一步提高系统性能，延长探测长度。

参　考　文　献

[1] Kawasaki B S, Hill K O, Johnson D C. Optical time domain reflectometer for single-mode fiber at selectable wavelengths[J]. Applied Physics Letters, 1981, 38(10): 740-742.

[2] Barnoski M K, Rourke M D, Jensen S M, et al. Optical time domain reflectometer[J]. Applied Optics, 1977, 16(9): 2375-2379.

[3] Blank L C, Spirit D M. OTDR performance enhancement through erbium fibre amplification[J]. Electronics Letters, 1989, 25(25): 1693-1694.

[4] Zhu N H, Tong Y W, Chen W, et al. Improved wavelength coded optical time domain reflectometry based on the optical switch[J]. Optics Express, 2014, 22(12): 15111-15117.

[5] Eickhoff W, Ulrich R. Optical frequency-domain reflectometry in single-mode fibers[J]. Applied Physics Letters, 1981, 39(3): 693-695.

[6] Soller B J, Gifford D K, Wolfe M S, et al. High resolution optical frequency domain reflectometry for characterization of

components and assemblies[J]. Optics Express, 2005, 13(2): 666-674.
[7] Venkatesh S, Sorin W V. Phase noise considerations in coherent optical FMCW reflectometry[J]. Journal of Lightwave Technology, 1993, 11(10): 1694-1700.
[8] Yuksel K, Wuilpart M, Mégret P. Analysis and suppression of nonlinear frequency modulation in an optical frequency-domain reflectometer[J]. Optics Express, 2009, 17(7): 5845-5851.
[9] Geng J H, Spiegelberg C, Jiang S B. Narrow linewidth fiber laser for 100-km optical frequency domain reflectometry[J]. IEEE Photonics Technology Letters, 2005, 17(9): 1827-1829.
[10] Ding Z Y, Yao X S, Liu T G, et al. Long measurement range OFDR beyond laser coherence length[J]. IEEE Photonics Technology Letters, 2013, 25(2): 202-205.
[11] Venkatesh S, Sorin W V. Phase noise considerations in coherent optical FMCW reflectometry[J]. Journal of Lightwave Technology, 1993, 11(10): 1694-1700.
[12] Amann M C. Phase noise limited resolution of coherent LIDAR using widely tunable laser diodes[J]. Electronics Letters, 1992, 28(18): 1694-1696.
[13] von der Weid J P, Passy R, Mussi G, et al. On the characterization of optical fiber network components with optical frequency domain reflectometry[J]. Journal of Lightwave Technology, 1997, 15(7): 1131-1141.
[14] Liu Q W, Fan X Y, He Z Y. Time-gated digital optical frequency domain reflectometry with 1.6-m spatial resolution over entire 110-km range[J]. Optics Express, 2015, 23(20): 25988-25995.
[15] Wei F, Lu B, Wang J, et al. Precision and broadband frequency swept laser source based on high-order modulation-sideband injection-locking[J]. Optics Express, 2015, 23(4): 4970-4980.
[16] Hotate K, Yamauchi T. Fiber-optic distributed strain sensing system by Brillouin optical correlation domain analysis with a simple and accurate time-division pump-probe generation scheme [J]. Japanese Journal of Applied Physics, 2005, 44(7L): L1030-L1033.
[17] Fan X Y, Koshikiya Y, Ito F. Phase-noise-compensated optical frequency domain reflectometry with measurement range beyond laser coherence length realized using concatenative reference method[J]. Optics Letters, 2007, 32(22): 3227-3229.
[18] Qin J, Shi H X, Xie W L, et al. Precise linearization of broadband frequency chirp for coherent optical frequency domain reflectometry[J]. Proceedings of SPIE, 2015, 9619: 96190A.
[19] Takada K. High-resolution OFDR with incorporated fiber-optic frequency encoder[J]. IEEE Photonics Technology Letters, 1992, 4(9): 1069-1072.
[20] Passy R, Gisin N, von der Weid J P, et al. Experimental and theoretical investigations of coherent OFDR with semiconductor laser sources[J]. Journal of Lightwave Technology, 1994, 12(9): 1622-1630.
[21] Ahn T J, Lee J Y, Kim D Y. Suppression of nonlinear frequency sweep in an optical frequency-domain reflectometer by use of Hilbert transformation[J]. Applied Optics, 2005, 44(35): 7630-7634.
[22] Hahn S L. Hilbert transforms in signal processing[M]. Boston: Artech House, 1996.
[23] Ang K H, Chong G, Li Y. PID control system analysis, design, and technology[J]. IEEE Transactions on Control Systems Technology, 2005, 13(4): 559-576.
[24] Chen D, Liu Q W, He Z Y. 108-km distributed acoustic sensor with 220-p/Hz strain resolution and 5-m spatial resolution[J]. Journal of Lightwave Technology, 2019, 37(18): 4462-4468.
[25] 刘铁根, 刘琨, 戴林, 等. 光电信息事件识别感知关键技术研究进展[J]. 光学学报, 2021, 41(1): 0106002.
Liu T G, Liu K, Dai L, et al. Research progress of key technologies in recognition sensing for opto-electronic information and event[J]. Acta Optica Sinica, 2021, 41(1): 0106002.
[26] 张旭苹, 丁哲文, 洪瑞, 等. 相位敏感光时域反射分布式光纤传感技术[J]. 光学学报, 2021, 41(1): 0106004.
Zhang X P, Ding Z W, Hong R, et al. Phase sensitive optical time-domain reflective distributed optical fiber sensing technology[J]. Acta Optica Sinica, 2021, 41(1): 0106004.

High Spatial Resolution TGD-OFDR Based on Internally Modulated DFB Laser

Dai Jianping[1], Qiu Jinbo[1], Liu Hongrui[1], Luo Yimin[1,2*], Liu Qingwen[2]

[1]*China Coal Technology and Engineering Group Shanghai Co. Ltd., Shanghai* 200030, *China*;

[2]*State Key Lab of Advanced Optical Communication Systems and Networks, Shanghai Jiao Tong University, Shanghai* 200240, *China*

Abstract

Objective An optical reflectometer is a powerful optical instrument, and it is widely adopted in distributed fiber optic sensors for loss location and temperature and stress measurement. Usually, optical reflectometers include optical time domain reflectometers (OTDRs) and optical frequency domain reflectometers (OFDRs). OFDR uses a sweeping laser as the light source. Compared with OTDR, it has higher spatial resolution and larger dynamic range. However, when the detection length is longer than the coherence length of the light source, the phase noise will degrade the system performance greatly. Meanwhile, a high spatial resolution requires a wide range of sweeps of the probe light. Because of the high cost of narrow linewidth lasers and modulators, OFDR is difficult to be commercialized at present. Therefore, most OFDR studies focus on phase noise and sweep ranges. There are already many ways to suppress OFDR phase noise, such as narrow linewidth lasers and coding and phase compensation algorithms. Time-gated digital optical frequency

domain reflectometry (TGD-OFDR) is also a method proposed in recent years to suppress phase noise and improve detection length. The frequency sweep method of OFDR is generally divided into external modulation and internal modulation. External modulation has better sweep performance and is easier to be controlled, but the sweep range is limited. The internal modulation has a large sweep range, but it has problems such as nonlinearity of the sweep frequency and linewidth broadening, and compensation or correction is often required through other means. Therefore, designing low-cost, long-range, and high-resolution TGD-OFDR systems is the main work in this paper.

Methods The TGD-OFDR system has the characteristics of a simple structure, which can effectively overcome phase noise and achieve long-distance detection. By taking the advantages of low cost, easy integration, and high sweep range of distributed feedback (DFB) lasers, an internally modulated DFB laser is selected as the swept frequency light source, and a TGD-OFDR system based on the DFB laser is designed. Firstly, by analyzing the modulation method and frequency sweep characteristics of DFB lasers, a pre-distortion system based on the Mach-Zehnder interferometer (MZI) and Hilbert variation of DFB laser sweep nonlinearity is designed. The system is a closed-loop feedback system and is divided into an optical path part and a circuit part. The optical path part is an MZI with a delay path, while the circuit part includes a computer-controlled acquisition card and an arbitrary waveform generator. In addition, the calculation of the Hilbert variation and proportion integral differential (PID) algorithms realizes the pre-distortion processing of the swept frequency. Secondly, the current-modulated DFB laser is used as the swept frequency light source, and it is proposed for demodulation. A frequency-stabilized laser is added as a local detection light. At the same time, due to the uncertainty of the frequency sweep rate of DFB lasers and the system characteristics of TGD-OFDR, a photodetector is added to receive the analog reference signal, and the analog reference signal is used as a matching filter to directly perform the cross-correlation algorithm to obtain the trace curve.

Results and Discussions In the demonstration reflectometry experiment, the duration of the pulse τ_p is set to 6 μs by an acoustic optical modulator. The pulse chirp range is about 1.1 GHz, corresponding to a theoretical spatial resolution of 9 cm. The local reference laser is a tunable single-frequency diode laser. A high speed analog to digital device (NI 5185) acquisition card with a sampling rate of 6.25 GSa/s and a resolution of 8 bit is used to sample the beat signal on the balanced photo detector. The fiber under test (FUT) is composed of three coils of single-mode fibers with a length of 24.7, 24.8, and 24.7 km, respectively. The measured trace is shown in Fig. 9(a). The dynamic range is measured to be 23.3 dB, and 2100 measurements at seven different laser wavelengths are carried out. The dynamic range can be further improved if the laser′s power is large. The spatial resolution at the start of the FUT is 10 cm, as shown in Fig. 9(b), which is very close to the theoretical spatial resolution. The spatial resolution at the far end of the FUT is about 18 cm, as illustrated in Fig. 9(c). The spatial resolution degeneration is mainly caused by the phase jitter of laser2 and the accumulation of phase noise, which is much larger than the linewidth of the DFB laser. Although the spatial resolution degenerates with a longer distance, it is still the best spatial resolution ever reported for the OFDR system with a measurement range of over 60 km.

Conclusions In this paper, an internally modulated DFB laser is used as the probe in the TGD-OFDR system. A frequency modulation range of up to 1.1 GHz with a fast modulation rate is achieved by using a current-modulated DFB laser, and a narrow linewidth diode laser is employed as the stable oscillator. A spatial resolution of 18 cm is realized over a fiber link of 74 km, which is believed to be the best resolution ever reported for the OFDR system of over 60 km. The system performance can be further improved by more precise pre-distortion algorithms, more stable oscillators, and stronger light source power.

Key words sensors; fiber measurement; time-gated digital optical frequency domain reflectometry; distributed feedback laser; pre-distortion